Infrared Spectroscopic Investigation of the Heterogeneous Reaction of HNO_3 and NaCl(100)

David Sporleder and George E. Ewing*

Department of Chemistry, Indiana University, Bloomington, Indiana 47405

Received: September 25, 2000; In Final Form: January 9, 2001

We have monitored the reaction of HNO_3 with the NaCl(100) faces of single crystals in the presence of minute water concentrations. The reaction produces $NaNO_3$ crystallites or ribbons atop the NaCl(100) face, indicating that a surface reorganization occurs upon exposure to water vapor concentrations as low as 0.02 mbar. The crystalline nature of the $NaNO_3$ is established by the well-defined longitudinal-transverse (LO-TO) splitting of the NO_3^- stretching vibrations. After an average coverage of 10 to 30 layers of crystalline $NaNO_3$, the reaction becomes diffusion limited, but shows no signs of stopping.

Introduction

Sea salt aerosol is among the most abundant particulate masses in the troposphere, existing as aqueous droplets or as solid particles under more arid conditions.[1,2] A possible link between the chloride ions of sea salt aerosol and tropospheric chlorine radicals has generated a considerable number of studies of the heterogeneous reactions of sodium chloride, the major component of sea salt, with trace atmospheric gases.[2] More specifically, it has been shown that oxides of nitrogen undergo the following reactions with NaCl.[3−18]

$$HNO_3(g) + NaCl(s) \rightarrow NaNO_3(s) + HCl(g) \quad (1)$$

$$2NO_2(g) + NaCl(s) \rightarrow NaNO_3(s) + ClNO(g) \quad (2)$$

$$N_2O_5(g) + NaCl(s) \rightarrow NaNO_3(s) + ClNO_2(g) \quad (3)$$

$$ClONO_2(g) + NaCl(s) \rightarrow NaNO_3(s) + Cl_2(g) \quad (4)$$

Reactions 2−4 yield gas-phase products with the potential to undergo photolysis and produce chlorine radicals. In turn, tropospheric ozone levels may be altered by the reactions of these radicals with O_3 or organics.[2] Interest in reaction 1 stems from its potential to compete with reactions 2−4.

Several kinetic and mechanistic studies of the reaction of nitric acid with sodium chloride have been performed.[3−5,7−10,13,14] The rate and extent of the salt conversion have been shown to increase in the presence of surface defects on the NaCl substrate and water vapor.[8,10,13,17] The reaction of $HNO_3(g)$ with a relatively defect free NaCl(100) surface produces a thin film of $NaNO_3$, 1−2 monolayers thick, under the extreme conditions of ultrahigh vacuum (UHV).[4,9,10] The reaction is self-limiting under these conditions, since the Cl^- ions become protected from HNO_3 vapor by the $NaNO_3$ layer. The thin film of $NaNO_3$ reorganizes into three-dimensional crystallites, sometimes by way of ribbons or strings,[14] on the NaCl surface upon exposure to pressures of water below the deliquescence point of either salt.[5,9,10,14,17] Thus, in the presence of water, the two salts separate. It has been shown that once this phase separation has occurred, fresh NaCl surface is present, and may further react with exposure to nitric acid.[5,9,10,14,17]

We report here a study of the reaction 1, nitric acid vapor with air cleaved NaCl(100) single-crystal faces, as monitored by Fourier transform infrared (FTIR) spectroscopy, with the goal of elucidating the reaction mechanism.

Experimental Section

The spectroscopic experiments performed in this work may be divided into four categories: spectroscopy of reactants and products, kinetic measurements, polarization measurements, and optical cross section determination.

A vacuum manifold that consisted of Pyrex, stainless steel, Teflon (stopcocks), and Viton O-ring seals, was employed to produce and introduce HNO_3 into the reaction cell. The pressure of the system was measured with a Baratron capacitance manometer (MKS Industries) for pressures greater than 10^{-3} mbar. Lower pressures were monitored with an ionization gauge (Vacuum Products, Inc.). The vacuum manifold was baked near 100 °C at a pressure of 10^{-5} mbar for no less than 20 h in order to reduce the amount of impurities absorbed on the walls.

The 10 cm reaction cell, described in detail elsewhere,[11] consists of two Pyrex cylindrical halves, which were connected by a Viton O-ring. The cell was soaked in a 1 M NaOH bath prior to being washed with deionized water and then dried with a heat gun. The purpose of this treatment was to remove any residual molecules absorbed on the Pyrex walls. Silicon windows (Infrared Optical Products, Inc.), which capped the cell, were used for two reasons. They are transparent over the wavenumber range of interest, and they are inert to nitric acid. In the kinetic experiments, two NaCl crystals (16 mm × 16 mm × 5 mm) with their (100) faces perpendicular to the propagation direction of the infrared radiation, were placed in the reaction cell. These samples were prepared by cleaving single crystals (Bicron and Atomergic Chemetals Corporation) along their (100) planes in a nitrogen purge tent.

The nitric acid source for the experiments was the vapor above a ternary mixture composed of 80 wt % H_2SO_4, 15 wt % H_2O, and 5 wt % HNO_3 and maintained at 273 K.[19] The mixture was prepared from a 95.8 wt % sulfuric acid solution (Fisher Scientific), 69.5 wt % nitric acid solution (Fisher Scientific), and deionized water. Successive freeze−pump−thaw cycles

* To whom correspondence may be addressed. Fax: (813) 855−8300. E-mail: ewingg@indiana.edu.

10.1021/jp0034729 CCC: $20.00
Published on Web 02/15/2001

were performed to degas the solution. Finally, the purity of the sample was tested by FTIR spectroscopy. A typical spectrum is shown in the results section.

Vibrational spectra were collected with an FTIR spectrophotometer (Nicolet Magna-IR 550). The transmitted light was detected with a liquid-nitrogen cooled mercury cadmium telluride (MCT) detector. A resolution of 4 cm^{-1} was used, and the 4000−650 cm^{-1} region was interrogated. A triangular apodization function was used to transform both the background and the sample interferograms for all experiments.

For the kinetic experiments, the NaCl crystals were sealed in the reaction cell, the vacuum manifold line was exposed to HNO_3 vapor in order to reduce loss of this reactant during the experiment due to deposition and reaction on the walls of the apparatus. The HNO_3 level was then brought to the desired pressure by manipulating the stopcock between the manifold and acid solution. To begin the reaction with the NaCl crystals, the stopcock connecting the reaction cell with the manifold was opened to introduce HNO_3 vapor. Reaction progress was monitored spectroscopically and fresh acid was introduced as necessary to maintain its constant pressure. Evacuating the cell, which permitted the collection of a final spectrum of only condensed phase species associated with the NaCl substrate, terminated the reaction.

For the polarization measurements, the incident radiation was polarized with a wire grid polarizer (Molectron), which was inserted between the reaction cell and the detector. The polarizer was used in conjunction with a single NaCl crystal canted at 30° so that the angle of radiation incidence could yield two distinct orientations of the electric field vector, E_s and E_p, relative to the (100) face of the salt.

Experiments to determine the optical cross section for NO_3^- utilized 1.2 and 0.59 M solutions prepared with reagent grade sodium nitrate (J. T. Baker, Inc) and deionized water. Pressing a drop between two zinc selenide windows (Spectral Systems) produced thin films of the aqueous solutions, of which FTIR spectra were taken.

Results

Spectroscopy of Reactants and Products. A typical absorbance spectrum of 0.2 mbar HNO_3 vapor in the 10 cm reaction cell without the NaCl crystals is shown in Figure 1. Several strong absorption bands are present that display the P, Q, and R branches of the HNO_3 fundamental vibrational modes as assigned by others.[20,21] Also observed are numerous weak features (absorbance ≤ 0.001) that can be attributed to overtone and combination bands of HNO_3.[20] Two regions of weak absorbances not due to nitric acid vapor are apparent. The 1617 cm^{-1} band, at the foot of the strong $HNO_3(\nu_2)$ absorption, is assigned to NO_2 vapor,[22] a known product of nitric acid decomposition,[23] which also can yield O_2 and H_2O. Multiple features in the 3600 to 4000 cm^{-1} region, more clearly evident on absorbance scale expansion, are the ν_1, ν_3 rovibrational bands of H_2O vapor. The corresponding vapor partial pressure, 0.02 mbar, was estimated by comparing the rovibrational absorbances with H_2O spectra of known pressure. Inspection of HNO_3 spectra of different pressures, revealed that spectra of higher acid pressures do not always contain more H_2O vapor. Thus, it is likely some of the water comes from another source, such as the walls of the manifold or reaction cell. The H_2O absorbance in Figure 1 was barely discernible from the noise; thus we take 0.02 mbar as an approximate lower detection limit for water vapor in our system.

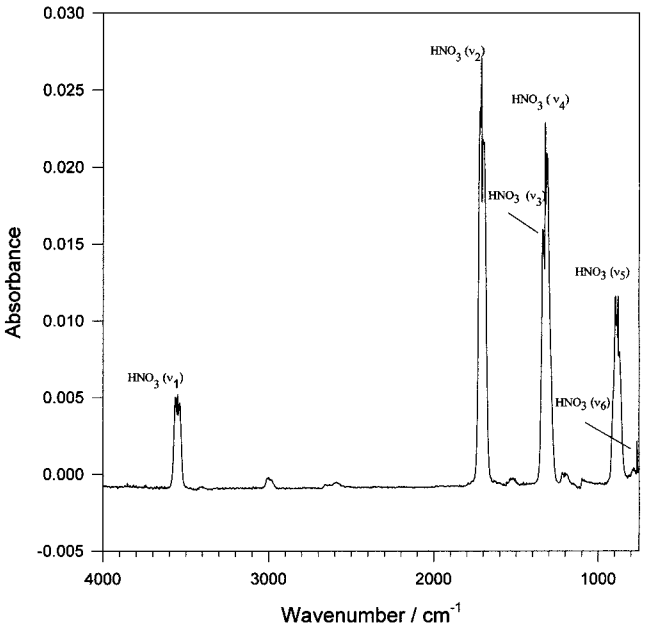

Figure 1. Absorbance spectrum of a 0.2 mbar HNO_3 (g) sample in the 10 cm reaction cell. The vibrational assignments are discussed in the text.

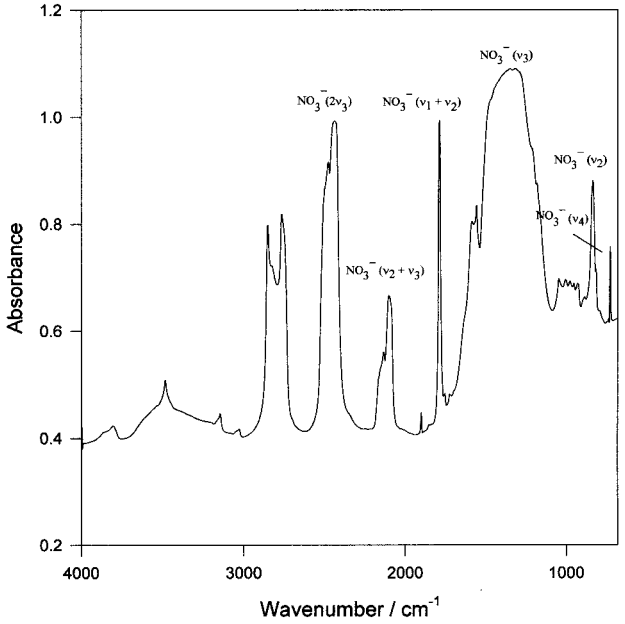

Figure 2. Absorbance spectrum of polycrystalline $NaNO_3$ formed from a drop of its saturated solution evaporated on a face of a NaCl crystal. The vibrational assignments are discussed in the text.

Figure 2 displays a spectrum of $NaNO_3$, produced by placing a drop of its saturated solution on the face of a crystal of NaCl and allowing the water to evaporate. The final product consisted of small rhombohedron crystals of $NaNO_3$, a few mm on a side, clearly visible on the NaCl substrate. Strong absorbances are assigned to fundamental bands, in accord with the study of James et al.[24] who examined transmission spectra of $NaNO_3$ optically dense single crystals. Other weaker features are suggested assignments of overtones and combinations of the fundamental vibrations.

A typical infrared absorbance spectrum collected during the course of a reaction of 0.34 mbar nitric acid vapor and two crystals of NaCl is shown in Figure 3a. It displays the progress of the reaction after 5.5 min. Features due to gas-phase HNO_3, consistent with the results in Figure 1, are highlighted with

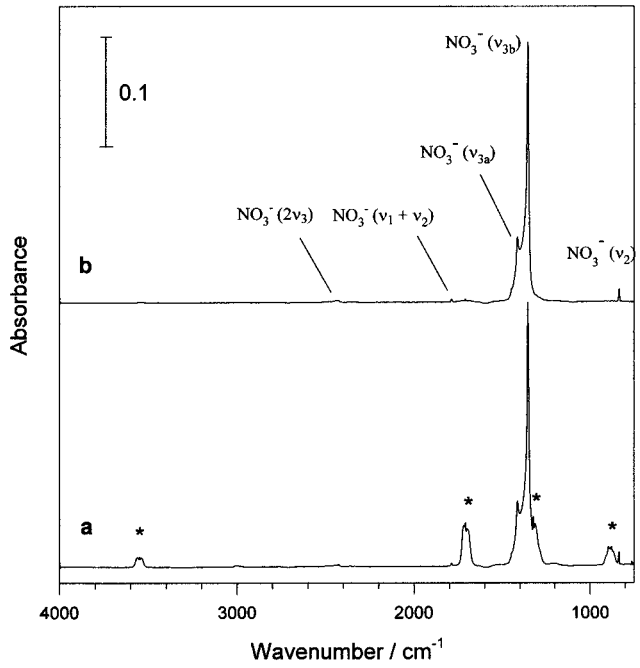

Figure 3. Absorbance spectra collected during the 5.5 min of the reaction of 0.34 mbar HNO_3 with the faces of two NaCl crystals. Spectrum a displays HNO_3 vapor absorbances marked by asterisks. The resulting NO_3^- features, after the HNO_3 gas-phase absorbance was subtracted out, is given in b.

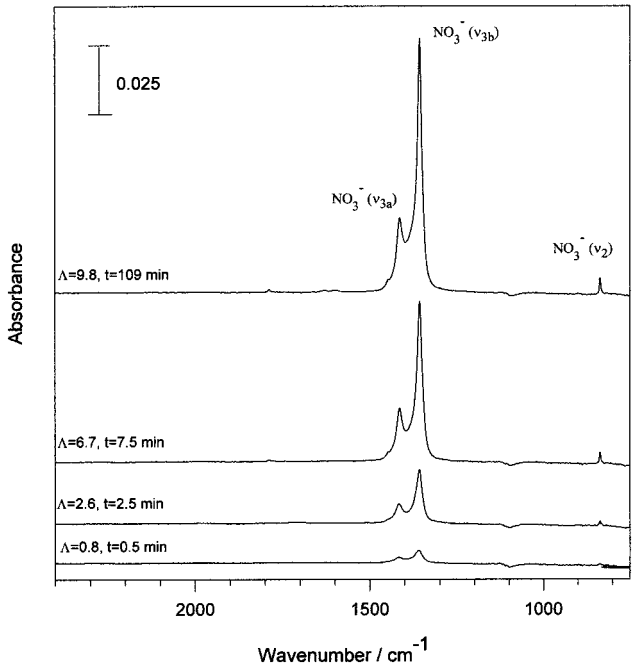

Figure 4. A sequence of spectra collected during the reaction of 0.026 mbar HNO_3 with the four faces of two crystals of NaCl. Contributions to the spectra due to HNO_3 have been removed. Assignments of the NO_3^- on the substrate are described in the text.

asterisks. The assignment of condensed phase nitrate vibrations, following other work,[5,11] are indicated in Figure 3b. The doublet features at 1415 and 1355 cm^{-1} are labeled as ν_{3a} and ν_{3b}, respectively. Weaker features match well with the overtone and combination bands in the polycrystalline $NaNO_3$ spectrum of Figure 2.

The other product formed by reaction 1 is gas-phase HCl identified by several of its well-known rovibrational features[25] near 3000 cm^{-1} that are clearly discerned on absorbance scale expansion. The HCl was only observed in the first two minutes of the 0.34 mbar HNO_3 reaction. We believe that the HCl is rapidly absorbed by the walls of the reaction cell, thus preventing its detection at other times.

To quantify the nitrate produced in the reaction the integrated absorbance of the ν_3 doublet was obtained. However, two nitric acid bands, ν_3 and ν_4, overlap with these absorbances. Thus, it was necessary to subtract out the HNO_3 features using a spectrum of pure HNO_3 (e.g., Figure 1) scaled to matching absorbances. The result of such a subtraction is shown in Figure 3b. Quantification of the nitrate formed will be discussed in a following section.

Kinetic Measurements. Presented in Figure 4 are infrared absorbance spectra for a reaction of 0.026 mbar nitric acid and the (100) faces of two NaCl crystals. For each of the individual spectra shown here, the HNO_3 vapor features were subtracted out. The only remaining absorbances are due to nitrate vibrations associated with the NaCl substrate. The reaction progress is quantified in terms nitrate production, reported as Λ, defined as the number of NO_3^- ions present for each initial Na^+Cl^- ion pair in the NaCl(100) face. Thus, Λ equal to one would be equivalent to a film of $NaNO_3$ one molecular layer thick covering the NaCl surface (assuming equal lattice constants). Although this definition of Λ is useful for thinking about the extent of the salt conversion, no interpretation pertaining to the arrangement of ions on the NaCl(100) surface is implied. We shall justify the quantification, Λ, in a later section.

Prior to the reaction, the nitrate features are absent. For the $\Lambda = 0.8$ spectrum, collected 0.5 min after the HNO_3 was introduced into the reaction cell, the doublet bands, ν_{3a} and ν_{3b}, are just visible at 1417 and 1360 cm^{-1}, and the ν_2 band is present at 836 cm^{-1}. (At 1100 cm^{-1}, the dip in the baseline that is the result of absorption by the Si windows not completely removed upon taking the ratio of the sample spectra with the background.)

The spectrum, collected after 2.5 min of the reaction, yields $\Lambda = 2.6$. The most obvious change is the increase in the nitrate doublet but, in addition, their absorbance ratio as well as their frequencies, now at 1416 and 1358 cm^{-1}, respectively, have changed slightly. Also, the ν_2 band has continued to grow. All three peaks have increased after 7.5 min of reaction as seen in the $\Lambda = 6.7$ spectrum. The nitrate doublet has shifted to 1414 and 1357 cm^{-1}.

The final spectrum in Figure 4 was taken 109 min after the initiation of the reaction, and the extent of salt conversion is $\Lambda = 9.8$. The doublet bands are located at 1414 and 1356 cm^{-1}.

The extent of salt conversion as a function of time and nitric acid pressures is presented in Figure 5. Five uptake curves at pressures ranging from 0.026 to 0.34 mbar HNO_3, are given. As indicated in the figure, two of these were studied with polarized light. All five pressures yield uptake curves of approximately the same shape, which we describe as having two growth regions. Note from Figure 5 that the lowest coverage detected is $\Lambda = 0.8$. A change in time scale beyond 40 min is provided to better reveal the long-term behavior of the NO_3^- production. The rapid initial rate of salt conversion we shall designate as region 1. Between 10 and 30 min, the growth slows. We designate the time dependence of the slower salt conversion as region 2.

The kinetic data are cast into an analytical form in a later section, the results of which are summarized in Table 1. We note for now that, as can be seen in Figure 5, the limiting coverage is not simply dependent on HNO_3 pressure. For example, runs in which the HNO_3 pressure is essentially the

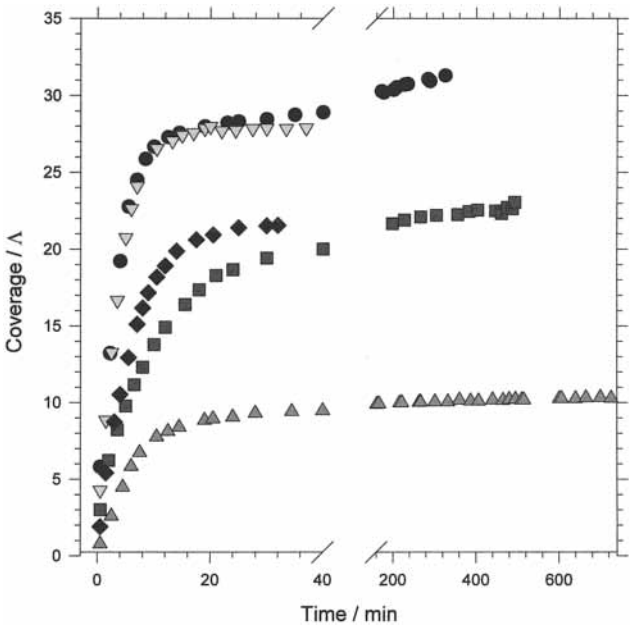

Figure 5. Growth of $NaNO_3$ on NaCl(100) at different HNO_3 pressures. The $NaNO_3$ coverage parameter, Λ, is defined in the text. The HNO_3 pressures are 0.026 mbar (triangles), 0.11 mbar (squares), 0.20 mbar, E_p (diamonds), 0.21 mbar, E_s (inverted triangles) and 0.34 mbar (disks).

TABLE 1: Values of Constants in $\Lambda = A(1 - e^{-bt}) + ct^{1/2} + d$ for Different HNO_3 Pressures in Its Reaction with NaCl(100)

HNO_3 pressure (mbar)	parameter A (Λ)	parameter b (s^{-1})	parameter c ($\Lambda s^{-0.5}$)	parameter d (Λ)
0.34	25	4.5×10^{-3}	0.027	2.0
0.21	27	4.5×10^{-3}	0.013	0.17
0.20	21	3.0×10^{-3}	0.026	0.063
0.11	17	1.7×10^{-3}	0.019	2.6
0.026	9.5	2.5×10^{-3}	0.0050	−0.13

same (0.20 and 0.21 mbar) yield values of Λ after 30 min that differ by 25%.

As expected, the absorbances of the fundamental vibration bands grow in unison throughout all of the reactions. However, the absorbance ratio of the two bands, which comprise the ν_3 doublet is not constant. Figure 6 shows how the ratio of peak absorbances of the ν_{3a} and ν_{3b} bands vary with coverage of nitrate on NaCl(100). Throughout the coverage range, the ratio of these absorbance peaks more than doubles.

Polarization Measurements. In an attempt to gain information on the arrangement of the NO_3^- ions on the surface, two different reactions were monitored using E_s or E_p polarized light for pressures of 0.21 and 0.20 mbar HNO_3 respectively with the (100) faces of one NaCl crystal canted 30° with respect to the propagation of the interrogation radiation. The NO_3^- absorptions grow in a manner similar to that found in the unpolarized spectra. Our results show that there are no discernible differences among the E_s, E_p, and unpolarized spectra. This statement is quantified in Figure 6.

Optical Cross Section. To determine the integrated optical cross section for the ν_3 doublet of NO_3^-, infrared absorbance spectra were collected for two aqueous solutions of nitrate. Figure 7 shows a spectrum of a thin film of 0.59 M $NaNO_3$ with principle features assigned.[26−28] Integrated absorbances of the ν_3 NO_3^- feature for 1.2 and 0.59 M solutions were found to be 17 and 8.0 cm^{-1} respectively. The calculation of the integrated cross section of ν_3 of the NO_3^- ion from these data is described in a following section.

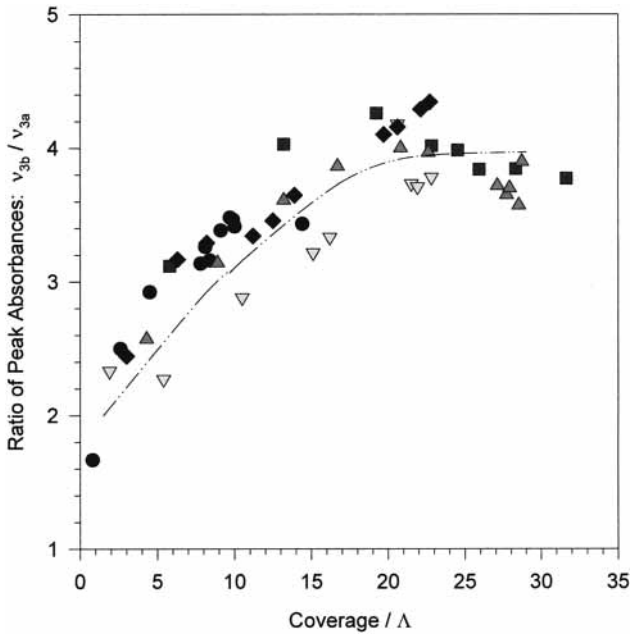

Figure 6. The ratio of peak absorbances of the two bands that comprise the ν_3 doublet is displayed as a function of the coverage parameter, Λ. The experiments that are not designated as either E_s or E_p were observed with unpolarized light. The line drawn through the data points serves only as a guide for the eye. The HNO_3 pressures are 0.026 mbar (disks), 0.34 mbar (squares), 0.21 mbar, E_s (triangles), 0.20 mbar, E_p (inverted triangles) and 0.11 mbar (diamonds).

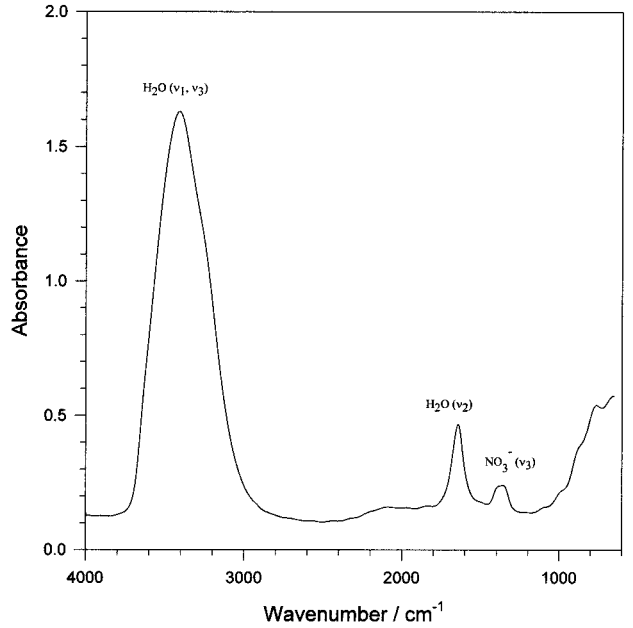

Figure 7. Absorbance spectrum of a thin film of 0.59 M $NaNO_3$.

Discussion

Spectroscopy Signatures. In Figure 8, we have collected a number of NO_3^- spectra in the ν_3 region from a variety of sources. Spectrum a is the absorption derived using optical constants obtained from reflection measurements from a face of single-crystal $NaNO_3$.[28,29] The middle spectrum, b, is transferred from Figure 3, a typical spectrum of nitrate produced by HNO_3 reaction on NaCl(100). Absorption by a thin film of a dilute $NaNO_3$ solution from Figure 7 is spectrum c.

We have purposely not transferred the ν_3 absorption in Figure 2, for the crystallites of $NaNO_3$ supported on the NaCl substrate, onto Figure 8. This feature is greatly distorted and its band shape

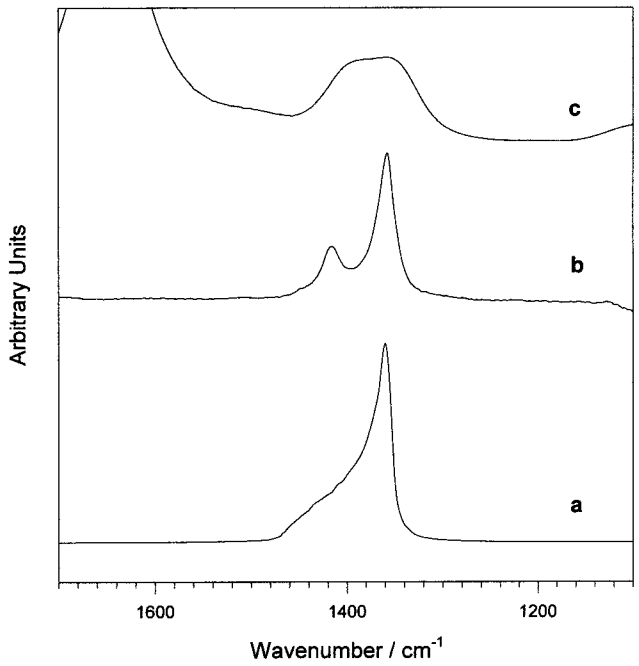

Figure 8. Spectroscopic signatures of the NO_3^- in different environments. In a, the absorbance of bulk $NaNO_3$ derived from optical constants of a single crystal.[28] In b, the absorbance of $NaNO_3$ formed by HNO_3 reaction with the NaCl(100) from this work. In c, the absorbance of 0.59 M aqueous $NaNO_3$ from this work.

is misleading. The reason is that the crystal sizes span a wide distribution. The larger ones are optically opaque in the ν_3 region, whereas the smaller ones absorb little. The net absorbance is a complicated convolution of this absorbing distribution of crystals. The spectrum is of value solely because it provides frequencies for the fundamental and overtone features.

It is perhaps surprising that the NO_3^- infrared signatures, as revealed by the three spectra of Figure 8, can be so different. To understand these differences and how they concern the theme of our study, we need to explore the symmetry of the NO_3^- ion and in its various condensed phases. The isolated ion is planar and belongs to the D_{3h} point group.[22] It has five infrared active modes: the nondegenerate ν_2 (a_2'') out-of-plane bending vibration at 831 cm^{-1}; the degenerate ν_3 (e') antisymmetric stretching vibrations at 1390 cm^{-1}; and the degenerate ν_4 (e') in-plane bending vibrations at 720 cm^{-1}. An infrared inactive mode, ν_1 (a'_1), the symmetric stretching vibration, is at 1050 cm^{-1}. In keeping with previous discussion of nitrate spectra produced by nitrogen oxides reacting with NaCl,[5,11] the spectroscopic labels in Figures 2−4 were made as if the NO_3^- ion were isolated.

We now turn our focus to the splitting of the ν_3 (e') transition into ν_{3a} and ν_{3b} that we observe for $NaNO_3$ on NaCl(100), in the hope of gaining insight on the environment in which the anion is located. Several possible explanations will be considered.

Absorption by molecules at different substrate sites can lead to splitting of even nondegenerate vibration bands. The reason this might occur is that heterogeneous environments, such as steps, edges, vacancies, and terraces, can perturb molecular vibrations in different fashions, resulting in frequency shifts. The bands attributed to different absorption sites would certainly have different binding energies, causing their relative intensities to change with coverage. Initially, absorbates would bind with the thermodynamically favored site until a large portion of these became occupied, allowing for absorption at the other sites. Although in our work, the relative intensities of the ν_3 doublet of NO_3^- on NaCl do change with coverage, this explanation is not favored based on the following observations. One, if the doublet component were due to different absorption environments then the ν_2 and $\nu_1 + \nu_2$ vibrations would likely be split as well. However, Figures 3 or 4 reveal these two bands as sharp singlets. Also, a coverage of more then a monolayer makes splitting due to different substrate sites unlikely. Assuming we have environmental spitting, once the NaCl face was covered with a layer of nitrate, the ν_3 doublet should stop growing since all of the absorption sites would be occupied and be replaced by another ν_3 absorption with its characteristic signature. On the contrary, Figure 4 shows that the ν_3 doublet continues to grow well after the formation of the first layer. Vogt and Finlayson-Pitts do attribute the splitting observed in their spectra of NO_3^- on NaCl to different absorption sites.[5] However, their salt substrate, pulverized crystals, and ν_3 frequencies are different from ours, so it is likely the arrangement of nitrate ions in their study is also different.

A second possible cause for the splitting of the $\nu_3(e')$ feature is a reduction in the symmetry of the NO_3^- ion. Peters and Ewing observed a doublet for NO_3^- on NaCl similar to ours, differing only in that both doublet features increased at the same rate.[11] They suggested that monomers, dimers, or other ordered arrays of nitrate ions associated with the NaCl surface result in lowering the D_{3h} symmetry to C_{2v} or C_1. This would lift the degeneracy of the ν_3 band into two IR active modes. However, the sharpness of the observed doublet features of NO_3^- on NaCl-(100), each bandwidth comparable to single-crystal $NaNO_3$ absorption (see Figure 8a), speaks against a collection of arrays of nitrate ions. Furthermore, Devlin et al. report that the ν_1 stretching vibration of NO_3^- monomers, dimers, and thin films is IR active.[31] There is no evidence of a ν_1 band, which should occur near 1050 cm^{-1},[22] in any of our spectra. Similarly, association of water molecules, possibly in the form of a hydrate, can reduce the symmetry of the NO_3^- ion. For example, infrared studies of dilute solutions of $NaNO_3$ by Irish and Walrafen[30] show a splitting of $\nu_3(e')$ into two overlapping features at 1405 and 1346 cm^{-1}. They assign these features $\nu_4(b_1)$ and $\nu_1(a_1)$, respectively, with spectroscopic labels in accord with the C_{2v} point group they propose for the NO_3^- ion solvated by water in the solution. Our spectrum in Figure 7, which also appears as spectrum c of Figure 8, is consistent with their results. We note that the positions of these solution doublet features are similar to those of NO_3^- on NaCl(100) as emphasized in comparing panels b and c of Figure 8. The $\nu_4(b_1)-\nu_1(a_1)$ difference of approximately 60 cm^{-1} for a variety of salts, on extrapolation to infinite dilution, is consistent with the view that solvated NO_3^- is in an environment that is essentially independent of the cations. However, at higher concentrations, the $\nu_4(b_1)-\nu_1(a_1)$ difference depends on the nature of the cation. As we have noted, water is present in our reaction cell. However if water is lowering the symmetry of each NO_3^- ion, this would require absorption in the ν_1, ν_3 region of liquid water. No such absorption is observed despite the large optical cross section in this region.[26,27]

A third type of splitting in solids, referred to as correlation field or factor group splitting, is the result of intermolecular coupling of internal vibrations between molecules within the same unit cell.[32,33] In this splitting, molecular vibrations couple with different phase relations of the other molecules in the unit cell. A vibration may be split into as many as n bands, where n is the number of molecules comprising the unit cell. The unit cell, see Figure 9, is rhombohedral and contains two $NaNO_3$

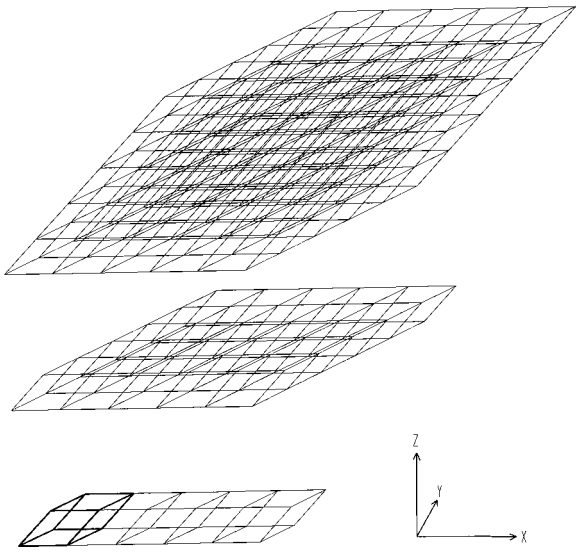

Figure 9. Crystallites of $NaNO_3$ as a needle, plate, and rhomboid. These crystallites are constructed by stacking unit cells of $NaNO_3$. A unit cell with $\alpha = 47°16'$ and $a_o = 631$ pm[34] is emphasized by the heavy lines to the left of the needle.

molecules.[34] The NO_3^- ions lie in parallel planes. The unit cell spectroscopic analyses of Eckhardt et al.[29] of the two nitrate groups show that the antisymmetric stretching vibrations that characterize the isolated ions, of type $\nu_3(e')$, couple to give two doubly degenerate vibrational modes. One, $\nu_3(e_u)$, is infrared active with transition dipoles directed orthogonal to the trigonal axis of the rhombohedral unit cell. The other, $\nu_3(e_g)$, is only Raman active. In spectrum a of Figure 8, the $\nu_3(e_u)$ mode is the prominent feature. Analogously, the $\nu_2(a_2'')$ NO_3^- bending modes couple in-phase to give the infrared active $\nu_2(a_{2u})$ mode along the trigonal crystal axis. The out-of-phase mode is the infrared inactive $\nu_2(a_{2g})$ mode. The resulting spectrum is the consequence of the coupling of transition dipoles of the unit cells that make up the (in principle) *infinite* crystal lattice. Since this coupling is limited to the unit cell by selection rules,[33] the size, shape or environment of the crystal does not come into play, so correlation field effects are not predicted to yield splittings. The isolated NO_3^- ion mode, $\nu_3(e')$, would become, in a macroscopic crystal, a singlet feature $\nu_3(e_u)$, and $\nu_2(a_2'')$ would become $\nu_2(a_{2u})$, also a singlet infrared absorption. We must look elsewhere for an explanation of the doublet features in the $\nu_3(e')$ region.

Finally, we consider longitudinal-transverse (LO-TO) splitting. It was first reported by Fox and Hexter that under certain conditions, the crystal shape can lower the overall environmental symmetry and lift degeneracies of infrared modes.[35] The conditions are satisfied by a crystal whose dimensions are much larger than the length of a unit cell, but much shorter than the wavelength of interrogating radiation. Also, the crystal shape must have at least one dimension much greater than the others. Vibrations of the coupled unit cells may be split into multiplets, as dipole−dipole interactions sum differently in the short and long directions. A single feature that results from the bulk crystal as in spectrum a of Figure 8, can be split when the crystal appears as a thin plate. This has been observed by Devlin et al.,[36] who prepared a thin crystalline plate of $NaNO_3$ on the surface of a substrate. Since their crystal was no longer a macroscopic extension of the rhombohedron, the C_3 axis of symmetry of the unit cell has been reduced to C_2 (or C_1) in the thin plate. The degeneracy of $\nu_3(e_u)$ that was made possible by the C_3 symmetry axis is thus lifted. The resulting frequencies found at 1450 and 1350 cm^{-1} correspond to a splitting more than double that we observe. Chang et al. observed LO-TO splitting for a thin plate of CO that epitaxially was grown on the NaCl(100) face.[37] In this case, the 3-fold degeneracy of a vibrational mode associated with the cubic unit cell of crystalline CO has been reduced by the symmetry of the thin plate. The transition dipole perpendicular to the NaCl(100) face (the LO mode) was detected by E_p light only. The transition dipoles parallel to the NaCl(100) face (the TO modes) are detected by both E_s and E_p polarizations. Because the LO and TO modes occur at different frequencies, the E_p and E_s spectroscopic profiles are different for the thin plate. In our system, the E_s and E_p spectra are identical so the directions of the transition dipole for the $NaNO_3$ crystals of our study must be qualitatively different than for thin plates of CO.

We have two levels of questions to explore with regard to $NaNO_3$ produced on the NaCl substrate. The first concerns the origin of the LO-TO splitting of the NO_3^- groups. The second asks about the orientation of the NO_3^- ions with respect to the NaCl(100) face.

Since the NO_3^- spectroscopic features are sharp and remain sharp for all coverages on the NaCl substrate, we shall assume that the $NaNO_3$ produced is crystalline as in Figure 8a. This is in contrast to the amorphous nitrate of the solution spectra, which gives rise to the diffuse bands of Figure 8c. Carrying this reasoning one step further, we shall take the crystalline $NaNO_3$ to be integral multiples of the rhombohedral unit cell.

Consider first the origin of the LO-TO splitting. Equal multiples of the unit cell stacked along *x* and *y* and *z* directions would produce macroscopic rhombohedral crystallites, which would be isotropic and yield *no* LO-TO splitting. This is illustrated in the upper portion of Figure 9 where 64 unit cells (5 on an edge) have been stacked. Likewise a stacking to produce a needle, as in the lower portion of Figure 9, would produce no LO-TO splitting. By contrast, thin plates, e.g., the middle panel of Figure 9, or any anisotropic stacking of the unit cell of $NaNO_3$ would lift the degeneracy of the $\nu_3(e_u)$ vibrations of the NO_3^- groups to produce a LO-TO splitting. We believe these sorts of irregularly shaped crystallites are responsible for the splittings we observe.

Next, we consider the alignment of the planar NO_3^- ions, or equivalently, the orientation of the unit cells on the NaCl(100) face. Consider a thin plate of an $NaNO_3$ crystal prepared by stacking rhombohedral unit cells flat against the NaCl(100) face, whereas in Figure 8, we take the *x*, *y* axes to lie in the NaCl-(100) plane. A little reflection shows, that in this configuration, each NO_3^- plane makes an angle of 15° with respect to the normal to the NaCl(100) surface. The corresponding $\nu_3(e_u)$ transition dipole along this 15° axis, and its partner of the LO-TO doublet in the NaCl(100) plane, would respond differently to E_s and E_p interrogations. Thus, a thin rhombohedral crystal of $NaNO_3$ flat against the NaCl(100) plane is incompatible with our polarization measurements. By contrast, an arrangement of plates of $NaNO_3$, canted such that the NO_3^- planes, make an angle of 45° with respect to the NaCl(100) plane, would satisfy the results of our polarization observations, which show no differences between E_s and E_p interrogations for the canted crystals. Moreover, measurements of the crystals orthogonal to the propagation direction of the radiation would give the same results. Finally, the $\nu_2(a_{2u})$ absorbance would appear as invariant with respect to the $\nu_3(e_u)$ doublet features in all the measurements. The proposed arrangement that yields NO_3^- planes canted at 45° with respect to the NaCl(100) face may seem unreasonably arbitrary. However, this arrangement is equivalent

to NO_3^- planes parallel to NaCl(111) planes. In NaCl(111), the trigonal arrangement of ions is compatible to the trigonal symmetry of the $NaNO_3$ unit cell axis. Thus, the growth of $NaNO_3$, as it replaces the substrate, may proceed along NaCl-(111) planes. A zigzag pattern of ribbons or strings of $NaNO_3$, such as has been observed in AFM experiments of NaCl(100) exposed to HNO_3 vapor,[14] would not be inconsistent with the equivalence of the E_s and E_p signatures we find. Alternatively, a random arrangement of rhombohedral microcrystals with one crystal axis shorter than the other two (to allow LO-TO splitting) could explain our spectroscopy.

Optical Cross Section. Now we consider the quantification of $NaNO_3$ production. Two different methods were employed to determine the integrated optical cross section of the ν_3 band of NO_3^-, one for $NaNO_3$ single crystals and the other for aqueous solutions of $NaNO_3$. The single crystal integrated cross section, $\bar{\sigma}$, was calculated from the imaginary index of refraction, $\kappa(\tilde{\nu})$, as summarized by Palik and Khanna[28] in the expression

$$\bar{\sigma} = \frac{4\pi}{\rho}\int_{\text{band}} \kappa(\tilde{\nu})\tilde{\nu}\,\mathrm{d}\tilde{\nu} \tag{5}$$

where ρ is the crystal molecular NO_3^- ion density,[34] and $\tilde{\nu}$ is the wavenumber with integration limits over the band 1250 to 1500 cm^{-1}. The result is $\bar{\sigma} = 3.0 \times 10^{-16}$ cm ion^{-1}. For the second method, the IR spectra of two aqueous solutions of $NaNO_3$ were used. Using the spectrum of Figure 7, for example, the integrated absorbance of the water bending mode, ν_2, together with its optical constants,[27] enabled the solution film thickness, 1.7 μm, to be determined. With the NO_3^- density in its aqueous solution, sample thickness, and integrated absorbance known, the calculation of $\bar{\sigma}$ by the Beer−Lambert expression is trivial. For $NaNO_3$ solutions of 0.59 and 1.2 M, we report cross sections of $3.2 \pm 0.2 \times 10^{-16}$ cm ion^{-1} and $3.4 \pm 0.2 \times 10^{-16}$ cm ion^{-1}, respectively. We find then that for both solid and aqueous states, the values of $\bar{\sigma}$ are, within experimental error, in agreement.

Peters and Ewing measured the NO_3^- optical cross section using the absorbance of a pressed pellet of 0.5% $NaNO_3$ in NaCl.[11] Their value differed by a factor of 7 from our determinations. We cannot account for the large discrepancy. Nonetheless, we prefer our value and contend that data of this kind obtained from single crystals or solutions are likely to be more reliable than that obtained from a pressed pellet.

Determination of Λ. One advantage of cleaved NaCl single crystals is that the initial surface area available for reaction is the geometric area of the crystals, and *S*, the surface density of 6.4×10^{14} Na^+Cl^- ion pairs cm^{-2}, is known.[38] The nitrate may be quantified from the ν_3 (or $\nu_3(e_u)$) integrated absorbance and the optical cross section for $NaNO_3$ single crystals. The Beer−Lambert expression[11]

$$\tilde{A} = \frac{nS\bar{\sigma}\Lambda}{\ln 10} \tag{6}$$

relates the surface coverage of NO_3^-, Λ, and its integrated absorbance, $\tilde{A}$. The integrated absorbance, given in wavenumbers, is measured from 1250 to 1500 cm^{-1}, to encompass the ν_3 NO_3^- absorption band. The number of NaCl (100) faces interrogated is expressed as *n*. Values of Λ so obtained appear throughout this paper.

Kinetics. Figure 10 displays the temporal dependency of salt conversion taken from Figure 5 for a pressure of 0.34 mbar HNO_3. Two distinct regions of growth can be identified. (The initial reaction on the *dry* sodium chloride surface was not observed because of traces of water present in our study. Scaling for our higher HNO_3 pressure, the H_2O-free measurements of Ghosal and Hemminger[17] would predict monolayer NO_3^- coverage in 10^{-2} s.) We begin to discuss the reaction in growth region 1. Figure 10 shows that this period of rapid growth occurs for about 10 min, to yield a Λ of about 25. It is important to note that more than just the surface Cl^- ions are available for reaction, as indicated by the large values of Λ. Finally, in region 2 there is a much slower rate of salt conversion, where Λ increases by only 10% over a 320 min period. Empirically, we have chosen the analytical expression

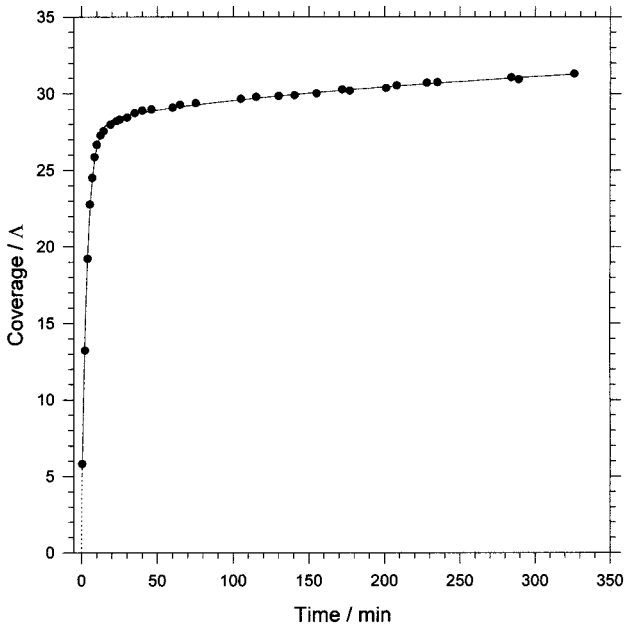

Figure 10. Coverage parameter of NO_3^- as a function of time. The closed circles are the data that give the extent of the NaCl conversion for the reaction of 0.34 mbar HNO_3 vapor. The solid line is the function $\Lambda = A(a-e^{-bt}) + ct^{1/2} + d$, used to quantify the coverage. The constants *a*, *b*, *c* and *d* are given in Table 1.

$$\Lambda = A(1 - e^{-bt}) + ct^{1/2} + d \tag{7}$$

to summarize the experimental data in regions 1 and 2 of Figure 10. In this equation, *t* represents the reaction time and *A*, *b*, *c*, and *d* are the constants adjusted to fit the experimental data. All of the growth curves in this study (e.g., Figure 5) are well described by this functional form. These constants for the various HNO_3 pressures are given in Table 1. Note that the region 1 increases exponentially with time and is described by the first term in the equation. Region 2 was found to increase with the square root of time as shown by the second term of the equation.

No consistent relationship between nitric acid vapor pressure and the growth rates was found. In fact, two runs at essentially the same pressure of HNO_3, 0.21 and 0.20 mbar, give significantly different values of the growth constants as indicated in Table 1. The sporadic rates and extents of reaction with HNO_3 pressure suggest that some aspect of our experimental condition is poorly defined. This uncontrolled variable, which effects the constants of the analytical expression of growth, is likely water. We have already shown in Figure 1, for example, that nitric acid in the reaction cell contains traces of water vapor and suggested that the likely source was the manifold walls. Thus, it is not unreasonable to postulate that water is always present in our reaction cell during each of the runs displayed in Figure 5. Works by Beichert and Finlayson-Pitts[8] and Davies and Cox[13]

have shown that the presence of water in reactions of NaCl powders and grains with nitric acid influences nitrate uptake. Also, Laux et al.[10] and Zangmeister and Pemberton[14] found that a NaCl(100) single-crystal face saturated with nitrate undergoes a surface reorganization upon the introduction of water vapor. Under certain conditions, ribbons or strings of $NaNO_3$ precede the formation of crystallites.[14] This surface reorganization exposes fresh NaCl surface (perhaps NaCl(111)?) which may react with HNO_3. Water present in trace concentrations could explain the varying rates and extent of reaction in our experiments.

Reaction Mechanism. Previously, it has been determined that the reaction of HNO_3 with a relatively defect free NaCl-(100) substrate produces a $NaNO_3$ film, 1−2 monolayers thick in the absence of H_2O.[4,9,10,18] This film passivates the NaCl surface preventing further reaction. However, in the presence of water vapor as low as 0.07 mbar, it was found that the $NaNO_3$ film reorganizes into three-dimensional crystallites, revealing fresh NaCl available for reaction.[5,9,10,14,17,18] This process requires a substrate that adsorbs water. In a recent study of water adsorption on well-defined NaCl(100), Foster and Ewing have measured the water adsorption isotherm under ambient conditions.[39] With vapor pressures of 0.1 mbar, an extrapolation of their water adsorption isotherm reveals an exceedingly small fractional coverage of 0.004. However, in the presence of HNO_3 vapor, the density of NaCl surface defects is likely to increase as the Cl^- ions are replaced by the NO_3^- ions. This change in surface structure would encourage water adsorption. Indeed, crystallites of NaCl, rich in defects, have been shown to enhance the water trapping efficiency of the surface by an order of magnitude.[40]

Ghosal and Hemminger recently presented a mechanism for surface nitrate formation under steady-state conditions and in the presence of adsorbed water.[17] Their mechanism is represented by two competing events: the adsorption of immobile nitrate ions that block adsorption sites on the NaCl surface and the freeing of these sites by H_2O induced recrystallization into three-dimensional $NaNO_3$ crystals. This presents us with a picture of the reacting surface as one that is constantly evolving, with three-dimensional crystals growing on a diminishing NaCl host crystal.

In the system studied here, it is likely the reaction initially produces nitrate ions adsorbed on the NaCl, which are immobile. This surface alteration enhances the adsorption of water molecules which serves to increase the ionic mobility of the surface. The nitrate ions are now free to migrate to form perhaps ribbons or strings[14] and then to the energetically favored state, $NaNO_3$ crystallites. All of these processes would take place in what we labeled region 1. The spectrum we have of the lowest coverage in region, $\Lambda = 0.8$, is shown in Figure 4. At this coverage, nitrate crystalline arrays have already formed as indicated by the doublet character of ν_3. We suppose, for $\Lambda = 0.8$, since ribbons or at least crystallites have formed, that the coverage is not uniform. Rather, the ribbons, many $NaNO_3$ unit cells thick, snake along defect sites leaving most of the NaCl-(100) surface not yet transformed. During the growth in region 1, the nitrate continues to adsorb as the surface is being reorganized, providing a constant source of NaCl available for reaction. Finally, coverages of $\Lambda = 10$ to 30 are achieved that translate to crystallites or ribbons with heights much greater.

A decrease in the reaction rate marks the start of the growth region 2. The $t^{1/2}$ dependence of the salt conversion in this region is indicative of random walk that characterizes gas-phase diffusion.[41] As the substrate surface becomes increasingly decorated with sodium nitrate ribbons or crystallites, less and less of it is available for further reaction. Also, as the ribbon or crystallite density increases, a warren of channels separates the HNO_3 from the unreacted NaCl surface. Gas-phase diffusion then becomes the rate-limiting step. Although nitrate production slows greatly, the reaction shows no signs of stopping in region 2. The changes in the relative absorbances of the ν_3 doublet features (see Figure 6) and their frequency shift with coverage is consistent with the growth of the crystallites since changes in their height, width and length ratios would alter the extent of dipole−dipole couplings possible that in turn affect LO-TO splittings.[35−37] Peters and Ewing suggested that gas-phase diffusion-limited the reaction of NO_2 with NaCl(100).[11] They interpret their results in terms of NO_2 diffusing into fractures in the NaCl substrate that were formed by the reaction itself. Perhaps here too it is the accumulated $NaNO_3$ crystallites or ribbons that finally slows the reaction by blocking the reacting gas from the NaCl substrate.

Conclusion

We have monitored the reaction of HNO_3 with the NaCl-(100) faces of single crystals in the presence of minute water concentrations. The reaction produces $NaNO_3$ crystallites or ribbons atop the NaCl(100) face, indicating that a surface reorganization occurs upon exposure to water vapor concentrations as low as 0.02 mbar. The crystalline nature of the $NaNO_3$ is established by the well-defined LO-TO splitting of the NO_3^- stretching vibrations. After an average coverage of 10 to 30 layers of crystalline $NaNO_3$, the reaction becomes diffusion limited, but shows no signs of stopping.

Acknowledgment. The authors thank the National Science Foundation through Grant No. ATM-9631838 for support of this research.

References and Notes

(1) Warneck, P. *Chemistry of the Natural Atmosphere*, 1st ed.; Academic Press: New York, 1988; Vol. 41.
(2) Finlayson-Pitts, B. J.; Pitts, J. N. Jr. *Atmospheric Chemistry: Fundamentals and Experimental Techniques*; John Wiley & Sons: New York, 1986.
(3) Fenter, F. F.; Caloz, F.; Rossi, M. J. *J. Phys. Chem.* **1994**, *98*, 9801.
(4) Laux, J. M.; Hemminger, J. C. *Geophys. Res. Lett.* **1994**, *21*, 1623.
(5) Vogt, R.; Finlayson-Pitts, B. J. *J. Phys. Chem.* **1994**, *98*, 3747.
(6) Timonen, R. S.; Chu, L. T.; Leu, M.-T.; Keyser, L. F. *J. Phys. Chem.* **1994**, *98*, 9509.
(7) Leu, M.-T.; Timonen, R. S.; Keyser, L. F. *J. Phys. Chem.* **1995**, *99*, 13 203.
(8) Beichert, P.; Finlayson-Pitts, B. J. *J. Phys. Chem.* **1996**, *100*, 15 218.
(9) Allen, H. C.; Laux, J. M.; Vogt, R.; Finlayson-Pitts, B. J.; Hemminger, J. C. *J. Phys. Chem.* **1996**, *100*, 6371.
(10) Laux, J. M.; Fister, T. F.; Finlayson-Pitts, B. J.; Hemminger, J. C. *J. Phys. Chem.* **1996**, *100*, 19 891.
(11) Peters, S. J.; Ewing, G. E. *J. Phys. Chem.* **1996**, *100*, 14 093.
(12) Fenter, F. F.; Caloz, F.; Rossi, M. J. *J. Phys. Chem.* **1996**, *100*, 1008.
(13) Davies, J. A.; Cox, R. A. *J. Phys. Chem. A* **1998**, *102*, 7631.
(14) Zangmeister, C. D.; Pemberton, J. E. *J. Phys. Chem. B* **1998**, *102*, 8950.
(15) Vogt, T.; Elliot, C.; Allen, H. C.; Laux, J. M.; Hemminger, J. C.; Finlayson-Pitts, B. J. *Atoms. Environ.* **1996**, *30*, 1729.
(16) De Haan, D. O.; Brauers, T.; Oum, K.; Stutz, J.; Nordmeyer, T.; Finlayson-Pitts, B. J. *Int. Rev. Phys. Chem.* **1999**, *18*, 343.
(17) Ghosal, S.; Hemminger, J. C. *J. Phys. Chem. A* **1999**, *103*, 4777.
(18) Hemminger, J. C. *Int. Rev. Phys. Chem.* **1999**, *18*, 387.
(19) Meyer, R. J. *Gmelins Handbuch der Anorganischen Chemie*; Verlag Chemie: Weinheim, 1963.
(20) McGraw, G. E.; Bernitt, D. L.; Hisatsune, I. C. *J. Chem. Phys.* **1965**, *42*, 237.
(21) Cohn, H.; Ingold, C. K.; Poole, H. G. *J. Chem. Soc.* **1952**, 4272.
(22) Herzberg, G. *Infrared and Raman Spectra of Polyatomic Molecules*; Van Norstrand Reinhold: New York, 1945; Vol. 2.

(23) Moeller, T. *Inorganic Chemistry*; John Wiley & Sons: New York, 1952.
(24) James, D. W.; Leong, W. H. *J. Chem. Phys*. **1968**, *49*, 5089.
(25) Herzberg, G. *Spectra of Diatomic Molecules*, 2nd ed.; Van Norstrand Reinhold: New York, 1950; Vol. 1.
(26) Walrafen, G. E. *J. Chem. Phys.* **1964**, *40*, 3249.
(27) Bertie, J. E.; Ahmed, M. K.; Eysel, H. H. *J. Phys. Chem*. **1989**, *93*, 2210.
(28) Palik, E. D.; Khanna, R. Sodium Nitrate ($NaNO_3$). In *Handbook of Optical Constants of Solids*; Palilk, E. D., Ed.; Academic Press: New York, 1998; Vol. 3; p 871.
(29) Eckhardt, R.; Eggers, D.; Slutsky, L. S. *Spectrochim. Acta* **1970**, *26A*, 2033.
(30) Irish, D. E.; Walrafen, G. E. *J. Chem. Phys*. **1967**, *46*, 378.
(31) Rowland, B.; Kadagathur, N. S.; Devlin, J. P. *J. Chem. Phys*. **1995**, *102*, 13.
(32) Sherwood, P. M. A. *Vibrational Spectroscopy of Solids*; Cambridge University Press: London, 1972.
(33) Decius, J. C.; Hexter, R. M. *Molecular Vibrations in Crystals*; McGraw-Hill Inc.: New York, 1977.
(34) Wyckoff, R. W. G. *Crystal Structures*, Vol. 2, pp 359−364, 2nd ed.; John Wiley & Sons: New York, 1964.
(35) Fox, D.; Hexter, R. M. *J. Chem. Phys*. **1964**, *41*, 1125.
(36) Devlin, J. P.; Pollard, P.; Frech, R. *J. Phys. Chem.* **1970**, *53*, 4147.
(37) Chang, H.-C.; Richardson, H. H.; Ewing, G. E. *J. Chem. Phys.* **1988**, *89*, 7561.
(38) Kittel, C. *Introduction to Solid State Physics*, 6th ed.; John Wiley & Sons: New York, 1986.
(39) Foster, M. C.; Ewing, G. E. *J. Chem. Phys* **2000**, *112*, 6817.
(40) Dai, D. J.; Peters, S. J.; Ewing, G. E. *J. Phys. Chem.* **1995**, *99*, 10299.
(41) Atkins, P. A. *Physical Chemistry*, 6th ed.; W. H. Freeman and Co.: New York, 1998.